nature climate change

LETTERS

PUBLISHED ONLINE: 17 APRIL 2017 | DOI: 10.1038/NCLIMATE3278

Energy budget constraints on climate sensitivity in light of inconstant climate feedbacks

Kyle C. Armour

Global energy budget constraints[1–3] suggest an equilibrium climate sensitivity around 2 °C, which is lower than estimates from palaeoclimate reconstructions[4], process-based observational analyses[5–7], and global climate model simulations[8,9]. A key assumption is that the climate sensitivity inferred today also applies to the distant future. Yet, global climate models robustly show that feedbacks vary over time, with a strong tendency for climate sensitivity to increase as equilibrium is approached[9–18]. Here I consider the implications of inconstant climate feedbacks for energy budget constraints on climate sensitivity. I find that the long-term value of climate sensitivity is, on average, 26% above that inferred during transient warming within global climate models, with a larger discrepancy when climate sensitivity is high. Moreover, model values of climate sensitivity inferred during transient warming are found to be consistent with energy budget observations[1–3], indicating that the models are not overly sensitive. Using model-based estimates of how climate feedbacks will change in the future, in conjunction with recent energy budget constraints[1,19], produces a current best estimate of equilibrium climate sensitivity of 2.9 °C (1.7–7.1 °C, 90% confidence). These findings suggest that climate sensitivity estimated from global energy budget constraints is in agreement with values derived from other methods and simulated by global climate models.

The response of Earth's climate to rising greenhouse gas concentrations remains a primary source of uncertainty in projections beyond several decades. One conceptually convenient and widely used metric of future warming is the equilibrium climate sensitivity (ECS)—defined as the global-mean near-surface air temperature change that would eventually result from a doubling of the atmospheric carbon dioxide (CO_2) concentration above pre-industrial levels. Although ECS cannot be measured directly, it can be estimated from a variety of methods[20], including simulation with climate models (encapsulating our physical theories of the climate system), palaeoclimate reconstructions[4], and observations of climate change over the past century[1–3,5–7,21–23].

Global energy budget constraints on ECS are compelling for their simplicity and direct use of historical climate records. Indeed, ECS is often derived[1–3,21–23] using only estimates of global surface warming, radiative forcing, and the rate of change in global heat content (ΔT, ΔF, and ΔQ, respectively) via the standard model of global energy balance[21],

$$\Delta Q = \Delta F - \lambda \Delta T \tag{1}$$

where the global radiative response ($\lambda \Delta T$) is assumed to increase linearly with global surface warming at a rate set by the net global climate feedback, λ; given the forcing from CO_2 doubling ($F_{2\times}$) a value for ECS is inferred as

$$\mathrm{ECS}_{\mathrm{infer}} = \frac{F_{2\times}}{\lambda} = \frac{F_{2\times}\Delta T}{\Delta F - \Delta Q} \tag{2}$$

Global energy budget analyses find a variety of values for $\mathrm{ECS}_{\mathrm{infer}}$, depending on their distinct estimates of ΔT, ΔF, ΔQ and $F_{2\times}$ (ref. 23; Table 1). The most recent studies[1–3] report best estimates around 2 °C, with a typical 5–95% confidence range of 1.1–4.0 °C. The implication[2] is that ECS may be at the low end of the ranges inferred from the palaeoclimate record[4] and process-based observational constraints[5–7], and below the range simulated by comprehensive global climate models (GCMs)—spanning 2.1 to 5.8 °C (Methods). Faced with divergent estimates, the Intergovernmental Panel on Climate Change's 5th Assessment Report revised the 'likely' lower bound on ECS downwards to 1.5 °C and concluded that no best estimate can currently be given[24].

The interpretation that observational estimates of $\mathrm{ECS}_{\mathrm{infer}}$ constrain the equilibrium climate sensitivity,

$$\mathrm{ECS} = \frac{F_{2\times}}{\lambda_{\mathrm{eq}}} \tag{3}$$

depends on a key, but often unstated, assumption: that the global climate feedback in operation when equilibrium is reached, λ_{eq}, will be equal to the feedback in operation at any given time, λ. However, there is growing theoretical and modelling evidence that this correspondence may not hold. Indeed, state-of-the-art GCMs show a strong tendency for λ to decrease over time—towards a less efficient radiative response to warming—as equilibrium is approached[9–18]. This behaviour appears to arise from the fact that the global radiative response depends not only on global surface warming, but also on the time-varying spatial pattern of warming[12,15,16]. For example, the Southern Ocean has shown little warming to date, but is expected to warm substantially over the coming centuries[13,25]; consequently, λ will tend to decrease in the future as destabilizing Southern Ocean feedbacks (for example, ice-albedo) become activated[12]. Evolving sea-surface temperature patterns also appear to drive changes in tropical cloud feedbacks that further cause λ to decrease over time[10,14–16,26]. As a result, $\mathrm{ECS}_{\mathrm{infer}}$ under transient warming is generally smaller than ECS. If nature behaves similarly, then global energy budget constraints on $\mathrm{ECS}_{\mathrm{infer}}$—based on observations of ΔT, ΔF and ΔQ—will also underestimate ECS (ref. 12). But by how much?

Because there are currently no observational constraints on how climate feedbacks will evolve in the future, estimates of ECS

School of Oceanography and Department of Atmospheric Sciences, University of Washington, Seattle, Washington 98195, USA. e-mail: karmour@uw.edu

Table 1 | Energy budget constraints on ECS_{infer} and ECS.

ECS_{infer} (°C); equation (2)	ECS (°C); equation (4)	ECS (°C); equations (4), (5)
2.5 (1.5–4.8)[1,19]	3.1 (1.9–6.1)	**2.9 (1.7–7.1)**
2.0 (1.2–3.9)[1]	2.5 (1.5–4.9)	2.3 (1.3–5.3)
1.64 (1.05–4.05)[2]	2.1 (1.3–5.1)	1.8 (1.1–5.5)
2.3 (1.6–4.1)[3]	2.9 (2.0–5.2)	2.7 (1.8–5.6)
3.0 (1.5–12.1)[22]	3.8 (1.9–15.2)	3.7 (1.7–∞)
6.1 (1.6–∞)[21]	7.7 (2.0–∞)	10.2 (1.8–∞)

(Left) Values of ECS_{infer} from equation (2) and values of ΔT, ΔF, ΔQ and $F_{2\times}$ reported by previous studies. (Middle) Estimates of ECS correcting for inconstant feedbacks using equation (4) with the CMIP5-mean value of λ/λ_{eq}. (Right) Estimates of ECS correcting for inconstant feedbacks using equations (4) and (5) with the CMIP5-mean value of $\lambda'/F_{2\times}$. Values are median and 90% confidence ranges, and any above 20 °C are reported as ∞. Bold values show the current best estimate of ECS reported in the main text, derived from values of ΔF, ΔQ and $F_{2\times}$ from ref. 1 with an updated estimate of ΔT from ref. 19.

cannot be made from observations alone. However, we can look to the climate models as a guide to how observed values of ECS_{infer} may be related to ECS. Here I use simulations from 21 GCMs participating in the most recent Coupled Model Intercomparison Project (CMIP5) to evaluate the ratio $\lambda/\lambda_{eq} = ECS/ECS_{infer}$. I then use this model-based estimate of λ/λ_{eq}, in conjunction with observations of ΔT, ΔF, ΔQ and $F_{2\times}$, to produce energy budget constraints on ECS that account for inconstant climate feedbacks via

$$ECS = \frac{\lambda}{\lambda_{eq}} \frac{F_{2\times}\,\Delta T}{\Delta F - \Delta Q} \quad (4)$$

This inconstancy of λ can be cleanly seen within abrupt CO_2 quadrupling simulations of the CMIP5 models[11,12,15] (Fig. 1a–c; see Methods). From equations (1) and (2), the relationship between the quantities $(\Delta F - \Delta Q)/F_{2\times}$ and $\Delta T/ECS$ reveals the value of λ/λ_{eq} (where the Δ values here are anomalies relative to the climate before

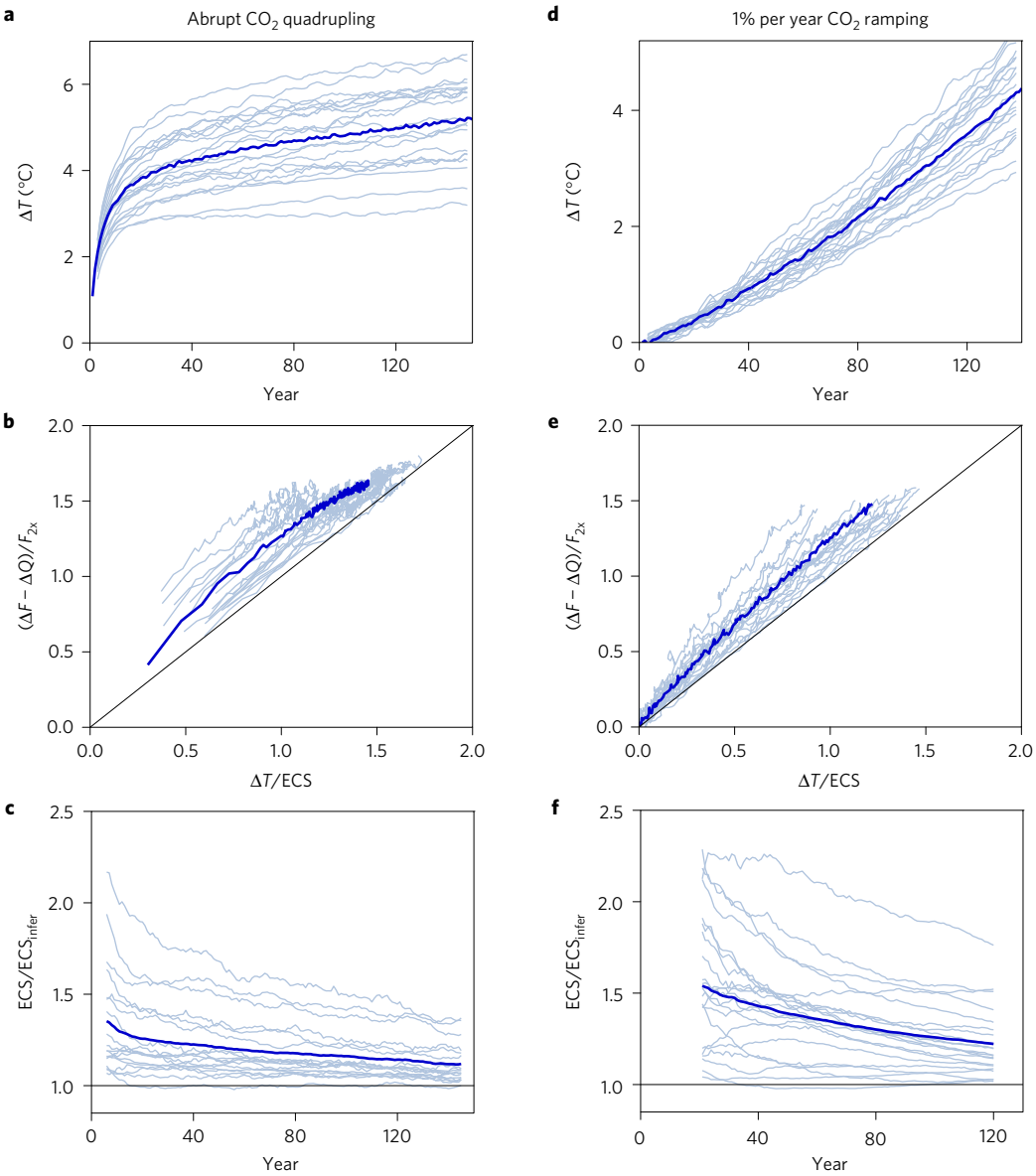

Figure 1 | Inconstancy of feedbacks in CMIP5 abrupt CO_2 quadrupling and 1% yr^{-1} CO_2 ramping simulations. a, Global-mean surface temperature anomaly over time. **b**, Global-mean surface temperature anomaly (normalized by ECS), plotted against global energy imbalance subtracted from radiative forcing (normalized by forcing from CO_2 doubling). **c**, The quantity $\lambda/\lambda_{eq} = ECS/ECS_{infer}$ over time. **d**–**f**, Same, but for 1% yr^{-1} CO_2 ramping. Light blue lines show individual models (5-yr running means for **a**–**e**, 31-yr running means for **f**); dark blue lines show CMIP5-mean.

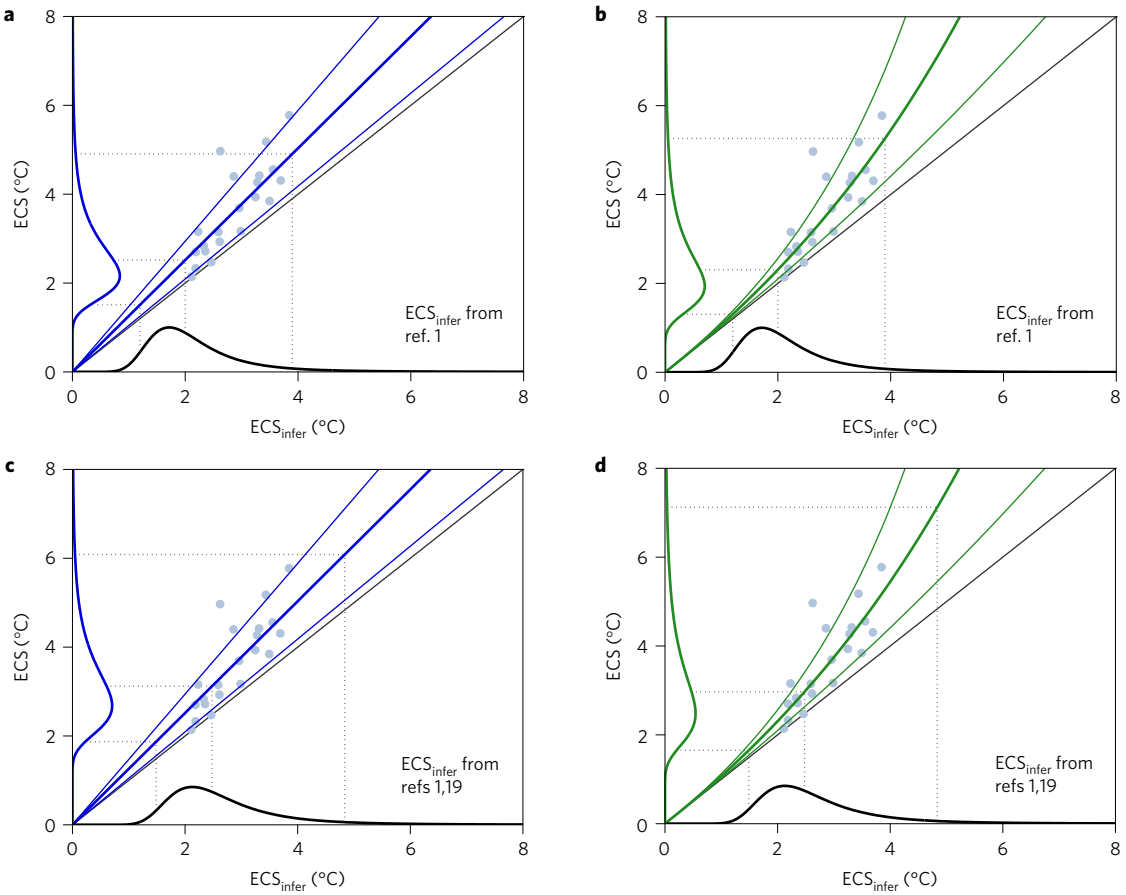

Figure 2 | Relationship between ECS and ECS$_{infer}$ for CMIP5 models, and comparison with energy budget constraints from ref. 1 (top) and refs 1,19 (bottom). a,**c**, Scatter plot of ECS against ECS$_{infer}$ for CMIP5 models (light blue points; Methods); all points lie on or above the one-to-one line, indicating ECS > ECS$_{infer}$. Thick blue line has slope equal to CMIP5-mean value of λ/λ_{eq} = ECS/ECS$_{infer}$ = 1.26, and thin blue lines have slopes equal to $\pm 1\sigma$ of λ/λ_{eq} across CMIP5 models. **b**,**d**, Same, but thick green curve through points shows λ/λ_{eq} = ECS/ECS$_{infer}$ calculated with equation (5) using the CMIP5-mean value of $\lambda'/F_{2\times} = 0.066\,^{\circ}C^{-1}$; thin green curves use $\pm 1\sigma$ of $\lambda'/F_{2\times}$ across CMIP5 models. Curves on axes show schematically how the probability density function of ECS$_{infer}$ is mapped to ECS for each case. Black curves on the *x* axes show ECS$_{infer}$ calculated using equation (2) and values from ref. 1 (top), or values from ref. 1 with the updated surface temperature from ref. 19 (bottom). Panels **a** and **c** use equation (4) with the CMIP5-mean value of λ/λ_{eq} to produce the blue curves on the *y* axis; Panels **b** and **d** use equations (4) and (5) with the CMIP5-mean value of $\lambda'/F_{2\times}$ to produce the green curves on the *y* axis; dashed lines show 5%, 50% and 95% percentiles.

CO_2 forcing). If λ were constant (equal to λ_{eq} at all times), then the GCMs would evolve along a constant slope of $\lambda/\lambda_{eq} = 1$ (the black line in Fig. 1b). While several do evolve nearly linearly, the majority follow a curved trajectory, with values of λ/λ_{eq} = ECS/ECS$_{infer}$ > 1 that decrease over time (Fig. 1b,c). In other words, there is a strong tendency for ECS to be larger than ECS$_{infer}$.

How does ECS/ECS$_{infer}$ behave under the more gradually increasing historical climate forcing? This question would ideally be addressed with historical simulations of the CMIP5 models, where realistic greenhouse gas, aerosol, and other climate forcings have been prescribed. However, historical forcing has been quantified accurately within only a few CMIP5 models[23,27]; most forcing estimates have been made[8] by prescribing a constant value of λ in equation (1), so cannot then be used to diagnose how λ changes over time. To overcome this limitation, I use the CMIP5 1% yr^{-1} CO_2 ramping simulations (Fig. 1d–f) as an analogue for slowly varying historical forcing. Within these simulations, the value of λ can be continuously diagnosed via equation (1) by making the approximation that radiative forcing increases linearly with time, reaching $F_{2\times}$ near year 70 (Methods).

Under 1% yr^{-1} CO_2 ramping, there is again a robust tendency for λ/λ_{eq} = ECS/ECS$_{infer}$ > 1 (Fig. 1e–f), with values typically greater than those in the same year following abrupt CO_2 quadrupling (compare Fig. 1c,f). This follows from the fact that the response to a linear forcing increase is, to a good approximation, equal to the sum of the responses to many incremental step increases in forcing: slowly increasing forcing continuously weights λ towards the higher values seen immediately following the abrupt CO_2 change. As a result, ECS/ECS$_{infer}$ decreases gradually—from about 1.5 to 1.2 over a hundred years, on average (thick line in Fig. 1f). Thus, the choice of year to use as analogue for changes under historical forcing does not have to be precise. Simulations with an energy balance model[9,28] that emulates the inconstant λ behaviour seen in CMIP5 models indicate that year 100 of the 1% yr^{-1} CO_2 ramping simulations provides the best estimate of ECS/ECS$_{infer}$ under historical forcing (Methods); results are similar if years 80 or 120 are used instead (Methods). At year 100, the CMIP5-mean value of λ/λ_{eq} = ECS/ECS$_{infer}$ is 1.26, meaning that ECS is about 26% higher than ECS$_{infer}$, on average. Yet there is a substantial spread across GCMs, with λ/λ_{eq} = ECS/ECS$_{infer}$ as low as 1.00 and as high as 1.89 (thin lines in Fig. 1f).

The relationship between values of ECS and ECS$_{infer}$ in CMIP5 models can be further explored by plotting one against the other (Fig. 2); all points lie on or above the one-to-one line (thin black lines), in closer agreement with a line with slope λ/λ_{eq} = 1.26 (thick blue lines in Fig. 2a,c) on average. The CMIP5 model range of ECS$_{infer}$ spans 2.1 to 3.8 °C. Importantly, all of the GCMs lie within

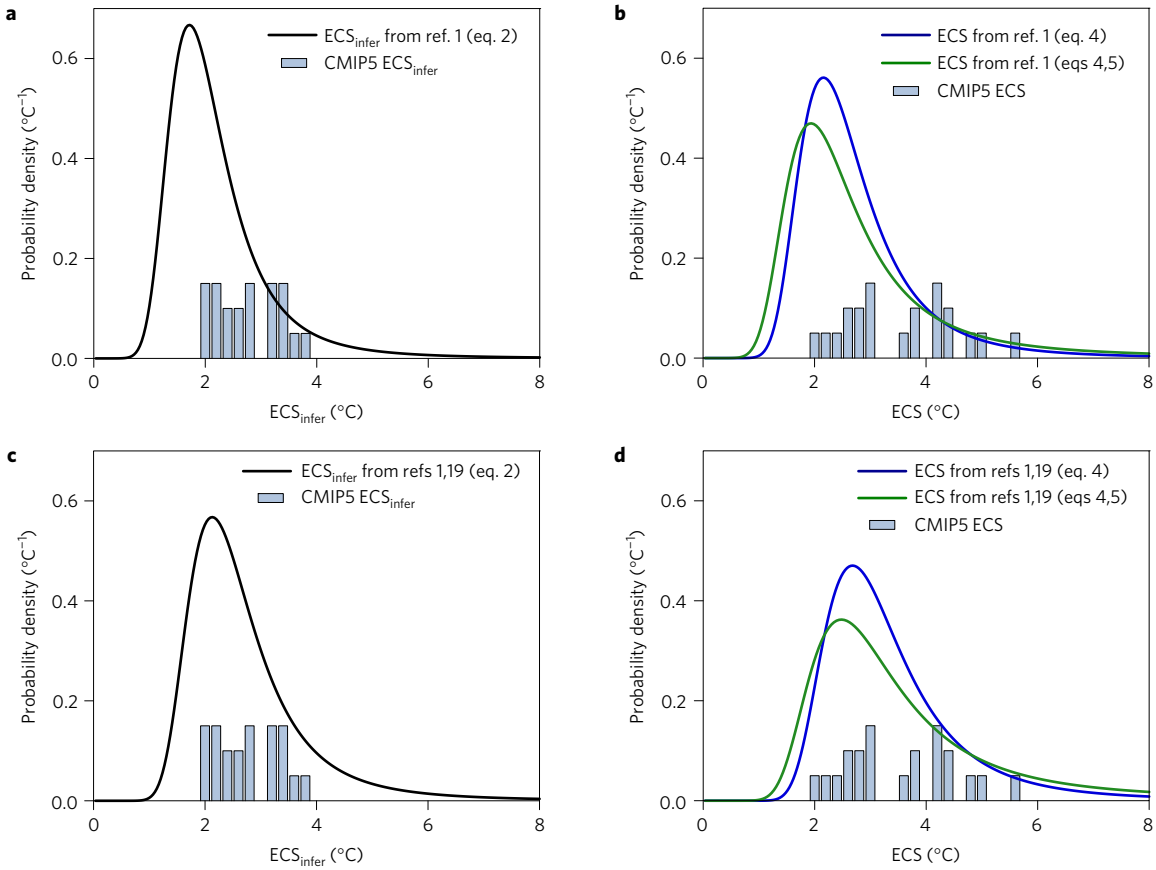

Figure 3 | Probability density functions of ECS$_{infer}$ and ECS derived from energy budget constraints from ref. 1 and refs 1,19, and comparison with CMIP5 models. a, ECS$_{infer}$ calculated using equation (2) and values of ΔT, ΔF, ΔQ and $F_{2\times}$ reported by ref. 1 (black curve, as in Fig. 2a,b). **b**, ECS derived from ref. 1 using equation (4) with the CMIP5-mean value of λ/λ_{eq} (blue curve, as in Fig. 2a) and using equations (4) and (5) with CMIP5-mean value of $\lambda'/F_{2\times}$ (green curve, as in Fig. 2b). **c**, ECS$_{infer}$ calculated using equation (2) and values of ΔF, ΔQ and $F_{2\times}$ reported by ref. 1 with updated value of ΔT from ref. 19 (black curve, as in Fig. 2c,d). **d**, ECS derived from refs 1,19 using equation (4) with the CMIP5-mean value of λ/λ_{eq} (blue curve, as in Fig. 2c and using equations (4) and (5) with the CMIP5-mean value of $\lambda'/F_{2\times}$ (green curve, as in Fig. 2d). Median values and 5–95% confidence range for each are given in Table 1 (**c**,**d**, first row and **a**,**b**, second row). Light blue bars show histograms of ECS$_{infer}$ (**a**,**c**) and ECS (**b**,**d**) values for CMIP5 models (Methods).

the observed 90% confidence range of ECS$_{infer}$ (thick black curves in Figs 2 and 3a,c), indicating that none are overly sensitive relative to global energy budget constraints. In other words, several GCMs appear too sensitive only when we misguidedly compare their values of ECS to observed values of ECS$_{infer}$.

The above results suggest that the range of ECS$_{infer}$ derived from energy budget constraints may be consistent with higher values of ECS. Using the CMIP5-mean value of $\lambda/\lambda_{eq} = 1.26$ in equation (4) suggests an ECS that is 26% higher than ECS$_{infer}$ (blue curves in Figs 2a,c and 3b,d; Table 1). However, this straightforward estimate neglects the possibility that λ/λ_{eq} itself might depend on the values of ΔT, ΔF, ΔQ and $F_{2\times}$. Indeed, a nonlinear relationship between ECS and ECS$_{infer}$ is expected from energy balance considerations: the timescale of climate response to forcing is longer when ECS is higher[29]; thus, for higher ECS the evolution towards equilibrium along a given curved trajectory in Fig. 1b,e will occur more slowly, leading to larger λ/λ_{eq} at any given time. The form of this relationship can be derived from the energy balance model[9,28] that emulates the inconstant λ behaviour of the CMIP5 models:

$$\frac{\lambda}{\lambda_{eq}} = 1 + (\lambda'/F_{2\times})\,\mathrm{ECS} = \frac{1}{1 - (\lambda'/F_{2\times})\,\mathrm{ECS}_{infer}} \quad (5)$$

where $\lambda' = \lambda - \lambda_{eq}$, and $\lambda'/F_{2\times}$ is independent of ECS (Methods).

For the CMIP5-mean value of $\lambda'/F_{2\times} = 0.066\,^{\circ}\mathrm{C}^{-1}$, equation (5) provides an improved fit to the CMIP5 values of ECS against ECS$_{infer}$ compared to the linear relationship (see Fig. 2a,b). Instead of ECS being uniformly 26% higher than ECS$_{infer}$, the ratio λ/λ_{eq} increases with ECS$_{infer}$ (Fig. 2b), giving: ECS = 1.3 °C for ECS$_{infer}$ = 1.2 °C (9% higher); ECS = 2.3 °C for ECS$_{infer}$ = 2.0 °C (15% higher); and ECS = 5.3 °C for ECS$_{infer}$ = 3.9 °C (36% higher). For higher values of ECS$_{infer}$, values of λ/λ_{eq} are higher still (Table 1). For example, ECS$_{infer}$ = 4.8 °C (the 95% confidence limit accounting for an up-to-date estimate of ΔT from ref. 19) corresponds to ECS = 7.1 °C (48% higher; Fig. 2d). This illustrates yet another reason why constraining the upper bound of ECS from transient climate observations is so challenging: if ECS is high, then climate is far from equilibrium and λ/λ_{eq} = ECS/ECS$_{infer}$ may be large.

Using equation (4) with the CMIP5-mean value of $\lambda'/F_{2\times}$ in conjunction with equation (5) with observed constraints on ΔT, ΔF, ΔQ and $F_{2\times}$ from Otto *et al.* (2013)[1] gives ECS = 2.3 °C (1.3–5.3 °C) (Figs 2b and 3b; Table 1)—higher than the reported[1] estimate of ECS$_{infer}$ = 2.0 °C (1.2–3.9 °C) based on equation (2). The values of ΔT, ΔF, ΔQ and $F_{2\times}$ given by Otto *et al.*[1] are specific to the years 2000–2009 relative to a 1860–1879 reference period; ECS derived from alternative values and periods are shown in Table 1. Using an up-to-date estimate of ΔT from Richardson *et al.* (2016)[19] (24% higher than reported in Otto *et al.*[1]) gives a best estimate of ECS$_{infer}$ = 2.5 °C (1.5–4.8 °C), corresponding to ECS = 2.9 °C (1.7–7.1 °C) (Figs 2d and 3d; Table 1). Current energy budget

estimates of ECS thus appear to be in agreement with those derived from other observational methods[4–7,20] and simulated by CMIP5 models (Fig. 3d).

The above estimates of ECS use only the CMIP5-mean value of λ/λ_{eq}, rather than accounting for the intermodel diversity in λ/λ_{eq} (thin lines in Fig. 2). This choice is based on the recognition that the CMIP5 range does not constitute a reliable representation of uncertainty, given interdependencies across models, and the fact that the ensemble is one of opportunity[30] rather than a systematic evaluation of possible λ/λ_{eq} values. Yet, if the GCMs showing high values of λ/λ_{eq} prove realistic, then ECS may be close to twice our observed values of ECS_{infer}; if it is instead the GCMs showing low values of λ/λ_{eq}, then ECS may be nearly equal to ECS_{infer}. A priority should thus be to identify the mechanisms driving the distinct inconstant λ behaviours across GCMs and, ultimately, to devise observational constraints. For now, the ranges of ECS reported here likely represent an underestimate of uncertainty, particularly at the upper bound (Methods).

Another target should be evaluating the extent to which the GCMs can capture the historical evolution of λ. Since λ appears to be sensitive to the spatial pattern of warming[12,15,16], the inability to simulate the observed pattern—whether due to deficiencies in forced response or simply internal variability—may bias model-based estimates of λ/λ_{eq}. Indeed, it appears that λ is largest while warming is delayed in the eastern tropical Pacific Ocean[15,26] and the Southern Ocean[10,12]—both regions that have shown cooling trends in recent decades that have proved challenging for GCMs to replicate[25]. To the extent that λ depends on the pattern of warming, this suggests that the estimates of λ/λ_{eq} reported here could be too low. Moreover, it is unclear to what extent changes in λ seen here under CO_2 forcing alone are related to those seen under different forcing agents, such as tropospheric aerosols that appear to drive even larger values of λ/λ_{eq} than does CO_2 (ref. 27); it is possible that the so-called 'efficacies' of different forcings may simply be another way of quantifying changes in λ arising from time-varying patterns of surface warming—thus, perhaps, already accounting for a portion of the λ/λ_{eq} behaviour identified here.

Energy budget constraints on ECS_{infer} will surely evolve in the future as estimates of ΔT, ΔF, ΔQ and $F_{2\times}$ continue to be updated. However, the principle discussed here will still apply: ECS may be substantially higher than energy budget estimates of ECS_{infer} suggest—provided that the behaviour of climate models, showing a robust tendency for climate feedbacks to change over time, is indicative of how nature will behave. For now, none of the CMIP5 GCMs appear overly sensitive relative to observed energy budget constraints when compared in a consistent way: a like-with-like comparison of ECS_{infer} with ECS_{infer}, rather than ECS with ECS_{infer} (Figs 2, 3). A challenge going forward is to rule out the possibility that very high values of ECS may be consistent with low values of ECS_{infer}, as a few of the GCMs suggest.

Methods

Methods, including statements of data availability and any associated accession codes and references, are available in the online version of this paper.

Received 16 September 2016; accepted 20 March 2017; published online 17 April 2017

References

1. Otto, A. *et al*. Energy budget constraints on climate response. *Nat. Geosci.* **6,** 415–416 (2013).
2. Lewis, N. & Curry, J. A. The implications for climate sensitivity of AR5 forcing and heat uptake estimates. *Clim. Dynam.* **45,** 1009–1023 (2015).
3. Kummer, J. R. & Dessler, A. E. The impact of forcing efficacy on the equilibrium climate sensitivity. *Geophys. Res. Lett.* **41,** 3565–3568 (2014).
4. Royer, D. L. Climate sensitivity in the geologic past. *Annu. Rev. Earth Planet. Sci.* **44,** 277–293 (2016).
5. Fasullo, J. T. & Trenberth, K. E. A less cloudy future: the role of subtropical subsidence in climate sensitivity. *Science* **338,** 792–794 (2012).
6. Sherwood, S. C., Bony, S. & Dufresne, J.-L. Spread in model climate sensitivity traced to atmospheric convective mixing. *Nature* **505,** 37–42 (2014).
7. Tan, I., Storelvmo, T. & Zelinka, M. D. Observational constraints on mixed-phase clouds imply higher climate sensitivity. *Science* **352,** 224–227 (2016).
8. Forster, P. M. *et al*. Evaluating adjusted forcing and model spread for historical and future scenarios in the CMIP5 generation of climate models. *J. Geophys. Res. Atmos.* **118,** 1139–1150 (2013).
9. Geoffroy, O. *et al*. Transient climate response in a two-layer energy-balance model. Part II: representation of the efficacy of deep-ocean heat uptake and validation for CMIP5 AOGCMs. *J. Clim.* **26,** 1859–1876 (2013).
10. Senior, C. A. & Mitchell, J. F. B. Time-dependence of climate sensitivity. *Geophys. Res. Lett.* **27,** 2685–2688 (2000).
11. Winton, M., Takahashi, K. & Held, I. M. Importance of ocean heat uptake efficacy to transient climate change. *J. Clim.* **23,** 2333–2344 (2010).
12. Armour, K. C., Bitz, C. M. & Roe, G. H. Time-varying climate sensitivity from regional feedbacks. *J. Clim.* **26,** 4518–4534 (2013).
13. Li, C., von Storch, J.-S. & Marotzke, J. Deep-ocean heat uptake and equilibrium climate response. *Clim. Dynam.* **40,** 1071–1086 (2013).
14. Rose, B. E. J. *et al*. The dependence of transient climate sensitivity and radiative feedbacks on the spatial pattern of ocean heat uptake. *Geophys. Res. Lett.* **41,** 1071–1078 (2014).
15. Andrews, T., Gregory, J. M. & Webb, M. J. The dependence of radiative forcing and feedback on evolving patterns of surface temperature change in climate models. *J. Clim.* **28,** 1630–1648 (2015).
16. Gregory, J. M. & Andrews, T. Variation in climate sensitivity and feedback parameters during the historical period. *Geophys. Res. Lett.* **43,** 3911–3920 (2016).
17. Knutti, R. & Rugenstein, M. A. A. Feedbacks, climate sensitivity and the limits of linear models. *Phil. Trans. R. Soc. A* **373,** 20150146 (2015).
18. Rugenstein, M. A. A., Caldiera, K. & Knutti, R. Dependence of global radiative feedbacks on evolving patterns of surface heat fluxes. *Geophys. Res. Lett.* **43,** 9877–9885 (2016).
19. Richardson, M. *et al*. Reconciled climate response estimates from climate models and the energy budget of Earth. *Nat. Clim. Change* **6,** 931–935 (2016).
20. Knutti, R. & Hegerl, G. C. The equilibrium sensitivity of the Earth's temperature to radiation changes. *Nat. Geosci.* **1,** 735–743 (2008).
21. Gregory, J. M. *et al*. An observationally based estimate of the climate sensitivity. *J. Clim.* **15,** 3117–3121 (2002).
22. Roe, G. H. & Armour, K. C. How sensitive is climate sensitivity? *Geophys. Res. Lett.* **38,** L14708 (2011).
23. Forster, P. M. Inference of climate sensitivity from analysis of Earth's energy budget. *Annu. Rev. Earth Planet. Sci.* **44,** 85–106 (2016).
24. IPCC *Climate Change 2013: The Physical Science Basis* (eds Stocker, T. F. *et al*.) (Cambridge Univ. Press, 2013).
25. Armour, K. C. *et al*. Southern Ocean warming delayed by circumpolar upwelling and equatorward transport. *Nat. Geosci.* **9,** 549–554 (2016).
26. Zhou, C., Zelinka, M. D. & Klein, S. A. Impact of decadal cloud variations on the Earth's energy budget. *Nat. Geosci.* **9,** 871–874 (2016).
27. Marvel, K. *et al*. Implications for climate sensitivity from the response to individual forcings. *Nat. Clim. Change* **6,** 386–389 (2015).
28. Held, I. M. *et al*. Probing the fast and slow components of global warming by returning abruptly to preindustrial forcing. *J. Clim.* **23,** 2418–2427 (2010).
29. Baker, M. B. & Roe, G. H. The shape of things to come: Why is climate change so predictable? *J. Clim.* **22,** 4574–4589 (2009).
30. Knutti, R. *et al*. Challenges in combining projections from multiple climate models. *J. Clim.* **23,** 2739–2758 (2010).

Acknowledgements

The author thanks T. Andrews, J. Bloch-Johnson, A. Donohoe, P. Forster, R. Knutti, C. Proistosescu, G. Roe and M. Rugenstein for enlightening discussions.

Additional information

Supplementary information is available in the online version of the paper. Reprints and permissions information is available online at www.nature.com/reprints. Publisher's note: Springer Nature remains neutral with regard to jurisdictional claims in published maps and institutional affiliations.

Competing financial interests

The author declares no competing financial interests.

Methods

CMIP5 simulations. The analysis includes all CMIP5 models (21 in total; listed in Supplementary Table 1) that provide output for near-surface air temperature and top-of-atmosphere (TOA) radiation fluxes for pre-industrial, CO_2 quadrupling and 1% yr^{-1} CO_2 ramping simulations. The CMIP5 variable names are 'tas' for near-surface air temperature, 'rsdt' for incoming TOA shortwave radiation, 'rsut' for outgoing shortwave radiation and 'rlut' for outgoing longwave radiation; net TOA radiation flux is calculated as rsdt−rlut−rsut.

To account for model drift, the linear trend over the corresponding years of each model's pre-industrial control simulations is removed from all variables for both CO_2 quadrupling and 1% yr^{-1} CO_2 ramping simulations. Anomalies in global-mean TOA radiation flux (ΔQ) and global-mean temperature (ΔT) are taken with respect to the (drift corrected) control simulations.

Following previous methods[15], ECS and $F_{2\times}$ within the CMIP5 models are estimated from the relationship between ΔQ and ΔT within the abrupt CO_2 quadrupling simulations (Supplementary Fig. 1). The linear regression over years 121–150 is extrapolated to $\Delta Q = 0$ (green lines in Supplementary Fig. 1) to estimate equilibrium warming; this value is then divided by two to estimate ECS for each model. Linear regression over years 1–5 is extrapolated to $\Delta T = 0$ (red lines in Supplementary Fig. 1) to estimate forcing from CO_2 quadrupling; this value is then divided by two to estimate $F_{2\times}$. The periods of years 1–5 and 121–150 are used to avoid the estimates of $F_{2\times}$ and ECS being biased by curvature in ΔQ versus ΔT, much of which occurs between these two periods[12]. CMIP5 values of ECS and $F_{2\times}$ calculated by this method (Supplementary Table 1) are in good agreement with those estimated via an alternative approach[9] that accounts for time-varying climate feedbacks but does not use regression. However, the values of ECS and $F_{2\times}$ tend to be higher than those estimated[6,8,31] from linear regression over years 1–150, which does not account for the effects of time-varying feedbacks. Values of λ_{eq} for each model are calculated via equation (3).

It is important to note that these values of ECS are derived from only 150 years of simulation, and thus may not be equal to the true equilibrium climate sensitivity values if the relationship between ΔQ and ΔT is nonlinear from the centennial timescale to equilibrium[12]. Those few CMIP5 models that have been run sufficiently long to reach equilibrium (for example, ref. 13) show that slope of ΔQ with ΔT tends to continue to flatten on millennial timescales, implying that the true values of ECS for some models may be slightly higher than those diagnosed here. Consequently, the values of λ/λ_{eq} reported here may be slightly lower than they would be if the true ECS values were known.

Radiative forcing within 1% yr^{-1} CO_2 ramping simulations is estimated using the approximation[32] $\Delta F(t) = F_{2\times}\log_2(C/C_0)$, where C_0 is the pre-industrial atmospheric CO_2 concentration and C is the concentration in year t of the ramping. For a 1% yr^{-1} (compounding) increase in CO_2 concentration, this gives:

$$\Delta F(t) \approx F_{2\times}\, t/69 \tag{6}$$

ECS_{infer} is calculated at each year of the 1% yr^{-1} CO_2 ramping simulations using equation (2) with values of ΔT, ΔF and ΔQ as 31-yr averages and with values of $F_{2\times}$ that are unique to each CMIP5 model. Values of ECS_{infer} shown in Figs 2, 3 and Supplementary Table 1 are calculated at year 100 of the 1% yr^{-1} CO_2 ramping simulations. Values of $\lambda' = \lambda - \lambda_{eq}$ for use in equation (5) are calculated via equations (1) and (3) with values of ΔT, ΔF and ΔQ as 31-yr averages. All CMIP5-mean calculations are performed using CMIP5-mean values of ΔT and ΔQ.

Energy balance model: equations and properties. A widely used[9,28,33] energy balance model (EBM) that captures the global-mean climate response to forcing simulated by the CMIP5 GCMs, including the time-dependent behaviour of global climate feedbacks, is governed by the following equations:

$$\begin{aligned} c_s \frac{dT}{dt} &= -\lambda_{eq} T + \varepsilon\gamma(T_d - T) + F \\ c_d \frac{dT_d}{dt} &= \gamma(T - T_d) \end{aligned} \tag{7}$$

where T is the change in global-mean surface temperature and T_d represents the temperature of the 'deep' ocean below the ocean mixed layer; c_s represents the effective heat capacity of the surface components of the climate system, approximately set by the depth of the ocean mixed layer[9]; c_d represents the effective heat capacity of the deep ocean below the mixed layer, approximately set by the depth of heat uptake under transient warming[33]; γ represents the strength of the coupling between the surface and deep ocean, related to the efficiency with which heat is vertically transported from the surface ocean to depth[33]; and ε represents the so-called ocean heat uptake efficacy, representing the dependence of global climate feedback on the time-evolving spatial pattern of ocean heat uptake[11,14,18,28].

The EBM successfully captures several fundamental properties of climate response common to all coupled GCMs, and can be tuned to accurately reproduce the unique response of each CMIP5 model to forcing (see refs 9,28,33). In particular, for mixed layer depths that are substantially shallower than the full ocean depth ($c_s \ll c_d$), the EBM captures the 'fast' and 'slow' (ref. 28) rates of global surface warming following abrupt CO_2 forcing (see Fig. 1a and Supplementary Fig. 2a)—corresponding to rapid warming of the surface components of the climate system followed by slow warming of the deep ocean.

Moreover, the EBM captures the inconstant λ behaviour simulated by the CMIP5 models (see Supplementary Fig. 2 and Fig. 1 and Supplementary Fig. 1). For global energy imbalance $Q = c_s dT/dt + c_d dT_d/dt$, equations (1) and (7) give

$$\lambda = \lambda_{eq} + (\varepsilon - 1)\,\gamma\left(1 - \frac{T_d}{T}\right) \tag{8}$$

Thus, the value of λ is distinct from λ_{eq} when ε and the ratio T_d/T are non-unitary. In the initial years following an abrupt CO_2 forcing, $T_d/T \approx 0$ and thus $\lambda = \lambda_{eq} + (\varepsilon - 1)\,\gamma$ (red line in Supplementary Fig. 2b); this captures the tendency of CMIP5 models to evolve along a line with slope that is steeper (more negative) than λ_{eq} in Q versus T space in the years following abrupt CO_2 quadrupling (red lines in Supplementary Fig. 1), corresponding to $ECS_{infer} < ECS$ when $\varepsilon > 1$ (Supplementary Fig. 2d). At times longer than the mixed layer adjustment timescale of a decade or so, the change in Q with T evolves according to $dQ/dt = \lambda_{eq}/\varepsilon$ (green line in Supplementary Fig. 2b); this captures the tendency of the CMIP5 models to evolve close to linearly in Q versus T space as equilibrium is approached (green lines in Supplementary Fig. 1), corresponding to slowly increasing ECS_{infer} when $\varepsilon > 1$ (Supplementary Fig. 2d). Finally, in equilibrium $T_d/T = 1$, giving $\lambda = \lambda_{eq}$ and $ECS_{infer} = ECS$.

It is interesting to consider why the EBM is able to capture the inconstancy of λ seen in the CMIP5 models[9]. The one-dimensional EBM represents changing λ in terms of two timescales with distinct radiative feedbacks: fast warming of the surface components of the climate system (over years), and slow warming of the deep ocean (over decades to centuries)[28]. Meanwhile, within the GCMs, λ appears to vary due to changing spatial patterns of surface warming[12,15] and/or ocean heat uptake[11,14,18] activating distinct radiative feedbacks: fast warming of the land, sea ice and the surface ocean except in the eastern Pacific Ocean and Southern Ocean (over years), and slow warming of the eastern Pacific Ocean and Southern Ocean (over decades to centuries)[15]. Thus, in one interpretation, the EBM is able to replicate the GCM behaviour simply because it captures a sufficient number of timescales of climate response associated with distinct feedbacks. However, another interpretation is that the EBM reflects the fact that the timescales of adjustment in the eastern Pacific Ocean and Southern Ocean should be similar to that of the deep ocean: warming in these regions is regulated by the rate at which water upwelled from depth is warmed itself[25]. More than two timescales would probably be needed if we were to consider longer GCM simulations that showed the relationship between ΔQ and ΔT evolving on timescales beyond several centuries (for example, allowing us to resolve the distinct timescales of response of the eastern Pacific and Southern oceans).

The EBM also yields an analytical form of λ/λ_{eq}. From equation (8),

$$\begin{aligned} \frac{\lambda}{\lambda_{eq}} &= 1 + (\varepsilon - 1)\,\gamma\left(1 - \frac{T_d}{T}\right)\frac{1}{\lambda_{eq}} \\ &= 1 + (\varepsilon - 1)\,\gamma\left(1 - \frac{T_d}{T}\right)\frac{ECS}{F_{2\times}} \\ &= 1 + (\lambda'/F_{2\times})\,ECS \\ &= \frac{1}{1 - (\lambda'/F_{2\times})\,ECS_{infer}} \end{aligned} \tag{9}$$

reported as equation (5) of the main text, where I have used the relation $ECS = F_{2\times}/\lambda_{eq} = \lambda/\lambda_{eq} ECS_{infer}$, and

$$\begin{aligned} \lambda' &= \lambda - \lambda_{eq} \\ &= (\varepsilon - 1)\,\gamma\left(1 - \frac{T_d}{T}\right) \end{aligned} \tag{10}$$

The value of λ' can be derived analytically. Under a linear increase in radiative forcing (that is, 1% yr^{-1} CO_2 ramping), $1 - T_d/T \approx c_d/(\gamma t) \times (1 - e^{-\gamma t/c_d})$, where terms of $\mathcal{O}(c_s/c_d)^2$ and higher order have been neglected for $c_s \ll c_d$ (see ref. 9 for full analytic solutions). This gives

$$\lambda' \approx \underbrace{(\varepsilon - 1)}_{\text{i}}\,\underbrace{\frac{c_d}{t}(1 - e^{-\gamma t/c_d})}_{\text{ii}} \tag{11}$$

In the initial years of the forcing increase (small t), term (ii) is approximately equal to γ and the expression reduces to $\lambda' = (\varepsilon - 1)\gamma$, which sets the greatest degree to

which λ can differ from λ_{eq}; λ' is large when the efficiency of deep ocean heat uptake γ and its efficacy ε are large. But term (ii) decreases over time, at a rate set by only ocean properties, rather than by value of ε or the equilibrium climate feedback λ_{eq}; it decreases slowly when heat uptake efficiency γ and the heat capacity the deep ocean c_d are large. Thus, λ' is large when ocean heat uptake is large, due to a high effective heat capacity of the climate system, in conjunction with high ocean heat uptake efficacy.

The behaviour of λ/λ_{eq} can be understood in a similar context. Its value is large when the climate system is far from equilibrium such that ocean heat uptake is high, which occurs when the effective heat capacity of the climate system is high (large γ and c_d); when the magnitude of the net climate feedback λ_{eq} is small (or, equivalently, ECS is high); and when the efficacy of that ocean heat uptake ε is large. Schematically, λ/λ_{eq} can be thought of as depending on both the degree of curvature in Q versus T space (Supplementary Fig. 2b) and the time it takes for the system to evolve along that trajectory.

In the main text, the form of equation (9) was used in conjunction with the CMIP5-mean value of $\lambda'/F_{2\times}$ under 1% yr^{-1} CO_2 ramping to calculate a CMIP5-mean estimate of λ/λ_{eq} (Fig. 2b,d). On the basis of these EBM results, the different values of $\lambda'/F_{2\times}$ across GCMs can be interpreted as arising from differences in their effective heat capacities, affecting how quickly they respond to forcing, and from differences in their ocean heat uptake efficacies (that is, how their climate feedbacks depend on the time-evolving pattern of heat uptake or surface warming).

Energy balance model: numerical simulations. Numerical simulations are performed of the EBM's global-mean temperature response to 1% yr^{-1} CO_2 ramping and historical forcing[34]. These simulations show that year 100 of 1% yr^{-1} CO_2 ramping provides an accurate estimate of ECS_{infer} over recent decades, and that updating values of ECS_{infer} by equations (4) and (5) produces a reliable estimate of ECS when applied to synthetic data.

EBM ocean parameter values (c_s, c_d, γ and ε) for the simulations are randomly drawn from uniform likelihood distributions with mean and range taken from fits[9] of the EBM to the response of the CMIP5 models to CO_2 quadrupling (Supplementary Table 2). To examine the EBM behaviour over a wide range of plausible climate sensitivities, ECS is drawn randomly from a uniform distribution between 1 and 15 °C; this corresponds to values of λ_{eq} between 3.44 and 0.23 W m^{-2} K^{-1} (assuming $F_{2\times}$ = 3.44 W m^{-2} as above).

A total of 50,000 simulations are performed with the EBM forced by the evolution of radiative forcing over 1765 to 2014 provided in the Representative Concentration Pathways (RCP)[34] (historical forcing until 2005 and its extension to 2014 with RCP8.5; data available at http://www.pik-potsdam.de/~mmalte/rcps). The time series of historical RCP aerosol forcing (RCP_{aero}) is rescaled to bring it in line with, and span the full range of uncertainty in, the IPCC estimate[35] of tropospheric aerosol forcing and its uncertainty in the year 2013 according to:

$$RCP_{aero}(yr) = RCP_{aero}(yr) \times \frac{IPCC_{aero}}{RCP_{aero}(2013)} \quad (12)$$

where $IPCC_{aero}$ = −0.9 W m^{-2} (−1.7 to −0.1 W m^{-2}, 90% confidence assuming Gaussian uncertainty). The CO_2 forcing is similarly scaled so that a doubling of the concentration corresponds to a forcing of $F_{2\times}$ = 3.44 W m^{-2} for consistency with the estimate from ref. 1.

Although the full range of EBM parameter values found in CMIP5 models is used, many of the parameter combinations are inconsistent with observed constraints on global surface warming, ocean heat uptake and radiative forcing. Thus, only those simulations (2,520 in total) that satisfy the condition:

$$\sqrt{\left(\frac{\delta T}{\sigma_T}\right)^2 + \left(\frac{\delta Q}{\sigma_Q}\right)^2 + \left(\frac{\delta F}{\sigma_F}\right)^2} < 1.65 \quad (13)$$

are kept, where δT, δQ and δF are the differences between global surface temperature, ocean heat uptake and total radiative forcing anomalies (mean over years 2000–2009 relative to mean over years 1860–1879) between the EBM simulation and observational estimates from ref. 1. The observational values are: $\Delta T_{obs} = 0.75 \pm 0.2$ °C, $\Delta Q_{obs} = 0.65 \pm 0.27$ W m^{-2}, $\Delta F_{obs} = 1.95 \pm 0.58$ W m^{-2} (5–95% confidence ranges); σ_T, σ_Q and σ_F in equation (13) each represent one standard deviation. The approach is thus one of Bayesian updating: the prior information is the range of EBM parameters given by the CMIP5 models and the aerosol forcing given by IPCC AR5; the prior is then updated based on historical climate observations. Note that while uniform priors have been criticized[36–38], the use of normal likelihood priors for the EBM parameters (using mean and standard deviation from ref. 9) here does not meaningfully change the results. An alternative choice of climate sensitivity prior would be a uniform distribution in λ_{eq} with values spanning 0.23–3.44 W m^{-2} K^{-1}, equivalent to a range of ECS over 1–15 °C but with a median value near 2 °C; this has the effect of selecting for lower values of ECS than does a prior that is uniform in ECS, but also does not meaningfully change the findings presented here with respect to the relationship between ECS_{infer} and ECS. Extending ECS beyond 1–15 °C makes little difference because values outside of this range are rarely able to satisfy the observational constraint (equation (13)).

The EBM historical simulations show a temperature response, that is, by design, in good agreement with the observed temperature record (Supplementary Fig. 3a). This is accomplished when the EBM parameter values, selected at random according to the distributions above, align favourably—for example, a high ECS paired with high aerosol forcing, high ocean heat capacity, or high ocean heat uptake efficacy (low ECS_{infer}). The probability density function of ECS for the simulations (dashed green curve in Supplementary Fig. 4b showing the true ECS distribution for all selected ensemble members) is given by 3.4 °C (1.9–8.7 °C, 90% confidence). However, ECS_{infer} calculated via equation (2) using anomalies over 2000–2009 is 2.6 °C (1.7–3.8 °C) (black curve in Supplementary Fig. 4b), close to the range of ECS_{infer} reported by ref. 1. The EBM simulations thus capture the tendency for low values of ECS_{infer} to be consistent with higher values of ECS as seen in CMIP5 models. Indeed, the value of $ECS/ECS_{infer} = \lambda/\lambda_{eq}$ under historical forcing is, on average, greater than one over the twentieth century; away from periods of rapid cooling associated with volcanic eruptions, its value decreases slowly over time (Supplementary Fig. 3c).

Another set of simulations are performed of the EBM response to 1% yr^{-1} CO_2 ramping by assuming a linear increase in forcing to a value $2F_{2\times}$ = 6.88 W m^{-2} in year 138 (Supplementary Fig. 3b); these simulations use only those parameter combinations that satisfy observed constraints as in Supplementary Fig. 3a, and thus have the same distribution of ECS as the historical simulations. The value of $ECS/ECS_{infer} = \lambda/\lambda_{eq}$ decreases slowly over time, consistent with the behaviour seen in the EBM historical simulations (Supplementary Fig. 3c) and the CMIP5 models forced by 1% yr^{-1} CO_2 ramping (Fig. 1f).

As in the main text, the probability density function of ECS can be estimated from ECS_{infer} under historical forcing using results of the 1% yr^{-1} CO_2 ramping simulations. To do so, periods of 1% yr^{-1} CO_2 ramping are selected so that the value of $ECS/ECS_{infer} = \lambda/\lambda_{eq}$ is most similar to that over years 2000–2009 of historical forcing; this occurs at year 100 of 1% yr^{-1} CO_2 ramping, when the respective values of ECS/ECS_{infer} are nearly perfectly correlated (Supplementary Fig. 3e).

At year 100 of 1% yr^{-1} CO_2 ramping, the EBM ensemble mean value of $\lambda'/F_{2\times} = 0.091\,°C^{-1}$ ($\pm 1\sigma = 0.061\,°C^{-1}$) is close to the value seen in the CMIP5 simulations in the main text. Using the form of equation (5) with a mean value of $\lambda'/F_{2\times}$ produces a good fit through the scatter plot of ECS against ECS_{infer} (Supplementary Fig. 4a). Correcting each ensemble member's value of ECS_{infer} using equation (5) with values of $\lambda'/F_{2\times}$ drawn randomly from an assumed normal likelihood distribution with the mean and standard deviation above produces an estimated ECS distribution (green curve in Supplementary Fig. 4b) of 3.4 °C (1.9–8.0 °C) that is a good approximation to the true ECS distribution (dashed green curve in Supplementary Fig. 4b).

Probability density functions. Following ref. 22, the probability density function (h) for ECS_{infer} (black curves in Figs 2 and 3a,c) is calculated via the relation:

$$h_{ECS_{infer}} = \int_0^\infty h_R h_T \left(\frac{ECS\,R}{F_{2\times}}\right) \frac{R}{F_{2\times}} dR \quad (14)$$

where $R = \Delta F - \Delta Q$; h_R and h_T are the probability density functions of observed[1] values of R and ΔT, respectively, which approximately follow normal distributions. The probability density function for ECS is calculated from equation (4) by rescaling $h_{ECS_{infer}}$ by the value of λ/λ_{eq}. The CMIP5-mean value of $\lambda/\lambda_{eq} = 1.26$ produces the blue curves in Figs 2a,c and 3b,d; a value of λ/λ_{eq} that varies with ECS_{infer} according to equation (5) and the CMIP5-mean value of $\lambda'/F_{2\times} = 0.066\,°C^{-1}$ produces the green curves in Figs 2b,d and 3b,d.

As illustrated in Fig. 2b,d, there is a range of $\lambda'/F_{2\times}$ across CMIP5 models ($\pm 1\sigma = 0.043\,°C^{-1}$) that was not taken into account in the estimates of ECS given in the main text. While the CMIP5 range cannot be treated as a formal estimate of uncertainty, a first-order estimate of the effect of uncertainty in $\lambda'/F_{2\times}$ can be obtained. To do so, a Monte Carlo simulation was performed wherein values of ΔF, ΔQ and $F_{2\times}$ are drawn randomly according to the normal likelihood distributions given in ref. 1 with updated ΔT from ref. 19 and convolved with equations (4) and (5), but with values of $\lambda'/F_{2\times}$ drawn from a normal likelihood distribution with mean and standard deviation as given by the CMIP5 models. The result is ECS = 2.9 (1.6–7.8) °C —slightly broader than the range of ECS estimated using only the CMIP5-mean value of $\lambda'/F_{2\times}$ in the main text, but with the same median value. The upper bound in particular has increased due to the form of equation (5): Gaussian uncertainty in $\lambda'/F_{2\times}$ leads to uncertainty in λ/λ_{eq} that is skewed towards higher values. The range of ECS reported in the main text should thus be interpreted as an underestimate of uncertainty, particularly at the upper bound.

Sensitivity of results to choice of year used to calculate ECS_{infer}. As shown in the main text, values of ECS_{infer} under 1% yr^{-1} CO_2 ramping decline slowly over time, suggesting that results do not depend sensitively on which year is used for the analysis. Using the CMIP5-mean value of $\lambda/\lambda_{eq} = ECS/ECS_{infer} = 1.26$ at year 100 in equation (4) gives ECS = 3.1 (1.9–6.1) °C for observed values of ΔF, ΔQ and $F_{2\times}$ from ref. 1 and ΔT from ref. 19 (see main text). If, instead, the CMIP5-mean value at year 80 or year 120 is used, the energy budget estimates of ECS change by only a small amount. At years 80 and 120, the CMIP5-mean values of λ/λ_{eq} are 1.31 and 1.22, corresponding to ECS of 3.2 (1.9–6.3) °C and 2.9 (1.8–5.9) °C, respectively. Using the CMIP5-mean value of $\lambda'/F_{2\times} = 0.066\,°C^{-1}$ in equations (4) and (5) gives ECS = 2.9 (1.7–7.1) °C (see main text). At years 80 and 120, the CMIP5-mean values of $\lambda'/F_{2\times}$ are $0.079\,°C^{-1}$ and $0.056\,°C^{-1}$, corresponding to ECS of 3.1 (1.7–7.8) °C and 2.9 (1.6–6.7) °C, respectively. Thus, the results in the main text are relatively insensitive to the choice of year used.

Data availability. The CMIP5 data were downloaded through the Program for Climate Model Diagnostics and Intercomparison's Earth System Grid (http://cmip-pcmdi.llnl.gov/cmip5/data_portal.html) and the Centre for Environmental Data Analysis (http://browse.ceda.ac.uk/browse/badc/cmip5). The data that support the findings of this study are available from the author upon request.

References

31. Andrews, T., Gregory, J. M., Webb, M. J. & Taylor, K. E. Forcing, feedbacks and climate sensitivity in CMIP5 coupled atmosphere-ocean climate models. *Geophys. Res. Lett.* **39,** L09712 (2012).
32. Myhre, G. *et al*. New estimates of radiative forcing due to well mixed greenhouse gases. *Geophys. Res. Lett.* **25,** 2715–2718 (1998).
33. Kostov, Y., Armour, K. C. & Marshall, J. Impact of the Atlantic meridional overturning circulation on ocean heat storage and transient climate change. *Geophys. Res. Lett.* **41,** 2108–2116 (2014).
34. Meinshausen, M. *et al*. The RCP greenhouse gas concentrations and their extension from 1765 to 2300. *Climatic Change* **109,** 213–241 (2011).
35. Myhre, G. *et al*. in *Climate Change 2013: The Physical Science Basis* (eds Stocker, T. F. *et al*.) 659–740 (IPCC, Cambridge Univ. Press, 2013).
36. Annan, J. D. & Hargreaves, J. C. On the generation and interpretation of probabilistic estimates of climate sensitivity. *Climatic Change* **104,** 423–436 (2011).
37. Lewis, N. An objective Bayesian improved approach for applying optimal fingerprint techniques to estimate climate sensitivity. *J. Clim.* **26,** 7414–7429 (2013).
38. Annan, J. D. Recent developments in Bayesian estimation of climate sensitivity. *Curr. Clim. Change Rep.* **1,** 263–267 (2015).